

Structural and optical property changes of zinc oxide nanopowders doped with cobalt and indium metals mechano-chemically

Mahlatse F. Manamela^{1*}, Thuto E. Mosuang^{1*}, Bonex W. Mwakikunga²

¹Department of Physics, University of Limpopo, University Road, Mankweng, Polokwane, 0727, South Africa.

²National Centre for Nano-Structured Materials, Council for Scientific and Industrial Research, University, Meiring Naude Road, Brummeria, Pretoria, 0001, South Africa.

*Corresponding author

DOI: 10.5185/amp.2018/401

www.vbripress.com/amp

Abstract

The mechano-chemical technique was employed to synthesise cobalt and indium single and double doped as well as the undoped ZnO nanopowder samples. The X-ray diffraction (XRD) and energy dispersive spectroscopy (EDS) results confirm that the prepared samples were of hexagonal wurzite form. A new peak was observed in the diffraction pattern of the In doped ZnO nanopowders. Doping the ZnO nanoparticles with Co and In did not significantly affect the lattice parameters, even though the average grain sizes were found to be reduced. The morphology of the samples revealed by the scanning electron microscopy (SEM) images appear to be more spherical. The excitation wavelength of 350 nm was used in the photoluminescence (PL) study where various defects related emissions were observed for the doped and undoped ZnO nanoparticles. The energy band gap of the prepared samples was calculated from the ultraviolet-visible spectroscopy (UV-Vis) data. It was found that the doped ZnO nanoparticles had smaller energy band gap compared to the undoped ZnO nanoparticles. The Raman experiment were performed at the excitation wavelength of 514.532 nm and E₂ (high) mode had the most intense peak. Copyright © 2018 VBRI Press.

Keywords: ZnO, Cobalt, indium, mechano-chemical, ball milling.

Introduction

Zinc oxide (ZnO) is a promising inorganic n-type semiconducting metal oxide. Its physical and optical properties are important for short-wavelength optoelectronic applications with a wide band gap of about ~3.3 eV [1]. This material enjoys superfluous advantage such as low cost, rich material source, non-toxicity and low temperature synthesis, as compared with other semiconductors like GaN and CuO [2, 3]. The investigations reveal that the crystal structure of a material hold routes to various applications [4]. ZnO has been found to have a large family of nanostructures including nanowires, nanorods, nanoballs, nanosheets and so on. The nano- scaled properties enhances the applications of manufactured macro- devices such as smart windows, gas sensors, solar cells, and ultraviolet light-emitters [5]. Djerdj et al. [6] investigated the ferromagnetic behaviour of ZnO nanoparticles, and obtained that they possess more strength when doped with Co metal. Literature reports by Donesha and Jayanna et al. [7] indicate that the crystal structure of ZnO does not change when co-doped by Fe and Co. Many methods are being developed in order to produce nanoparticles of controlled size, such as ZnO and TiO₂ nanoparticles [8, 9]. As such, sol-gel method, one of the well-known technique was used by Spanhel et al. [10] and Maswanganye *et al.* [11] to prepare zinc oxide nanoparticles.

The aim of this work is to study the structural and optical properties of ZnO nanoparticles prepared using high energy ball milling method. Further on the effect of Co and In doping and co-doping in the structural and optical reforms will be noted and analysed. This mechano-chemical method has been found to be adaptable and its processes can be followed easily.

Experimental

Materials details

Zinc oxide (99.9 %), cobalt (99.8 %) and indium (99.9 %) were purchased from Sigma-Aldrich and utilized in this study without any further purification.

Material synthesis

5% wt doped Co-ZnO and In-ZnO nanoparticles were synthesized mechano-chemically using an 8000 MIXER of ball milling machine for 12 hours. The double doping ZnO nanoparticles with two metals cobalt and indium was also performed for 2.5 % wt-indium and 2.5 % wt-cobalt to make 5% wt doping. This was attained by directly putting proportionate amounts of ZnO and (Co or In) for single (Co and In) for double doping into the steel vial together with two stainless steel balls of diameter 6.825 mm and ball milled for 12 hours.

Characterizations

The samples obtained were later characterized using the X-ray diffraction (XRD), scanning electron microscope (SEM), Raman spectroscopy (RS), photoluminescence (PL) and ultraviolet-visible (UV-vis) spectroscopy.

Results and discussion

X-ray diffraction (XRD)

The crystal structure of ZnO nanoparticles was investigated using XRD having incident Cu $K\alpha_1$ radiation ($\lambda=1.541 \text{ \AA}$). The XRD results were collected by scanning the samples with diffraction angle between $2\theta = 20$ and 60° in 0.02° steps. **Fig. 1.** displays an XRD pattern which exhibit several diffraction peaks that can be indexed as hexagonal wurtzite structure, since peaks at $2\theta = 31.77$, 34.43 , 36.27 , 47.56 and 56.63° belonging to the (100), (002), (101), (102) and (110) planes respectively (JCPDS No.36-1451) were observed. This implies that the Co^{+2} ions were successfully incorporated into the lattice position of Zn^{+2} ions. Looking at the XRD pattern of In-ZnO nanoparticles, a new peak along the (400) plane (*) was observed between 31.78° and 34.44° . This peak is associated with an indium dopant [12]. Speculations were that Co^{+2} prefers the interstitial site which leads to great stress in the structures when compared to filling in a Zn^{+2} vacancy of which In^{+3} seems to be preferring. The crystallite size, strain and lattice parameters of undoped ZnO, Co doped ZnO, In doped ZnO and Co-In doped ZnO are listed in **Table 1**. The results show the crystallite size of Co-ZnO nanoparticles being the largest of all the calculated nanoparticles, except for the purchased ZnO samples. When looking at the strains, the reverse was observed. The explanation could be extracted from the ionic radii of both In^{+3} and Co^{+2} . Since the ionic radius of Zn^{+2} is 0.60 \AA while that of In^{+3} is 0.62 \AA which is greater than that of Co^{+2} 0.58 \AA , then the In^{+3} changes the structure of ZnO more than Co^{+2} [13]. It can also be observed that the crystallite size of all the single doped ZnO nanoparticles are larger than those of the co-doped ZnO nanoparticles. Another fact is the crystallite sizes calculated using Debye-Scherrer's equation [14] are large compared to the ones calculated by Williamson-Hall equation [15]. This is caused by the contribution of the strain parameter calculation that is included in the Williamson-Hall equation and not in the Debye-Scherrer's equation. While the strain of single doped ZnO nanoparticles are smaller than those of co-doped ZnO nanoparticles. The percentage difference between the reported lattice parameters [16, 17] and the calculated ones are comparable.

Table 1. The calculated crystallite size (by Williamson-Hall and Debye-Scherrer), strain and lattice parameters of 5% doped and undoped ZnO.

Sample name	Debye-Scherrer (nm)	Williams on-Hall (D) (nm)	Strain (ϵ)	Parameters (\AA)	
				a=b	c
As-purchased ZnO	49.414	43.036	0.002	3.252	5.210
Undoped ZnO	18.258	16.080	0.006	3.251	5.208
Co-ZnO	21.791	18.804	0.005	3.250	5.207
In-ZnO	20.570	17.765	0.005	3.249	5.204
(Co-In) ZnO	15.354	13.263	0.006	3.254	5.211

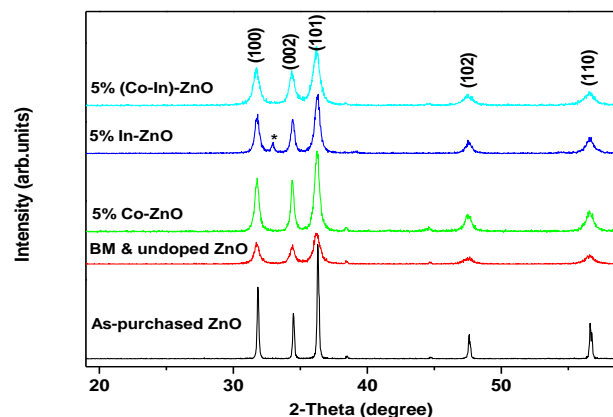


Fig. 1. XRD pattern of the undoped and 5% wt doped Co-ZnO, In-ZnO and (Co-In)-ZnO nanoparticles milled for 12hours.

Scanning Electron Microscopy (SEM)

The Joel [JSM-7500F] model of SEM was used to observe the morphology of the ZnO nanoparticles. The images were taken at 100 nm scale and a magnification of x50. The SEM images appear to be spherical in shape as shown in **Fig. 2.** (a) and (b) for undoped ZnO nanoparticles and co-doped ZnO nanoparticles. The morphology of the ZnO nanoparticles were not significantly affected by the dopants added.

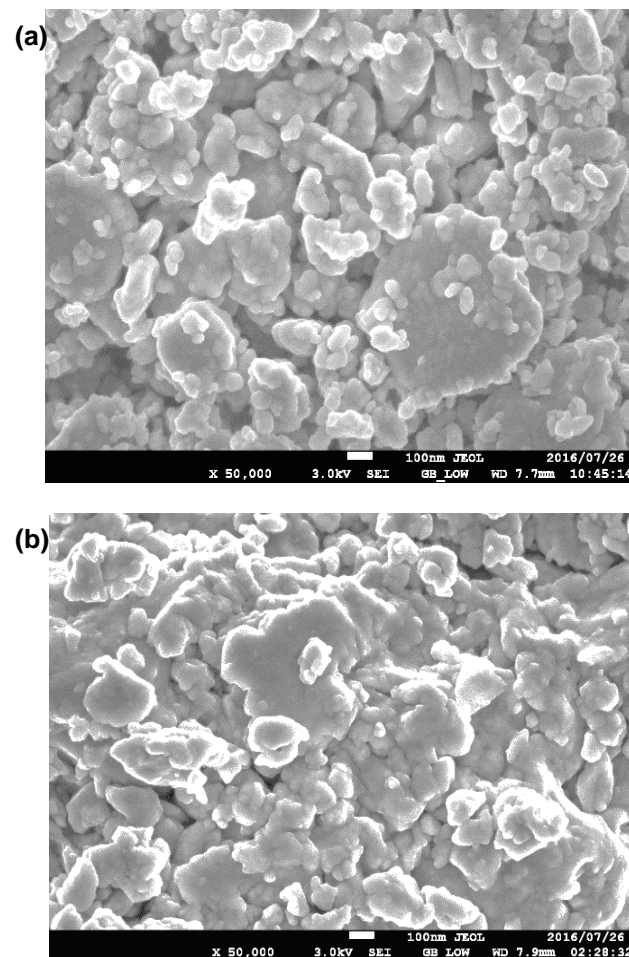


Fig. 2. (a) The SEM of undoped ZnO nanoparticles. (b) The SEM of 5% wt co-doped (Co-In)-ZnO nanoparticles.

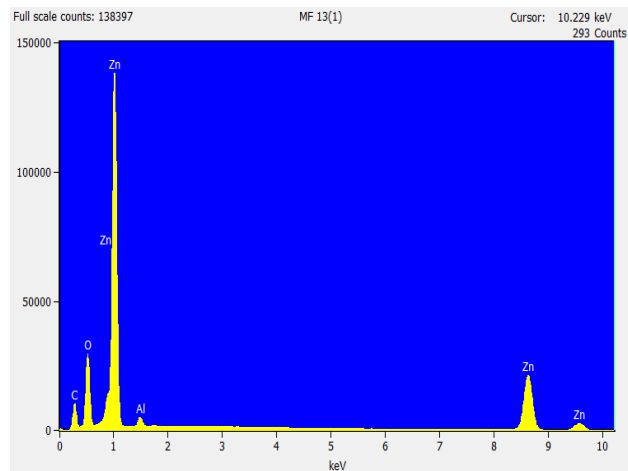


Fig. 3. The EDS of undoped ZnO nanoparticles.

The energy dispersive spectroscopy (EDS) shows all the elements present in the sample (Zn and O); see Fig. 3. for undoped ZnO nanoparticles. The elemental composition of the undoped ZnO nanoparticles was analysed and found to have Zn = 46.57, O = 26.90, C = 25.02 and Al = 1.51. The samples were mounted on carbon (C) tape, hence the presence of the weak C peak on the EDS spectra. The EDS of the undoped ZnO nanoparticles shows the presence of a peak that belongs to aluminium element. This was caused by the aluminium stab used when collecting data. There are several peaks for Zn in the EDS spectra as compared to other as ZnO was the host material.

Raman Spectroscopy (RS)

The Raman scattering method was employed to probe the vibrational modes and the phase purity of the ZnO nanoparticles. Fig. 4. shows the room temperature Raman scattering spectra of the doped and undoped ZnO nanoparticles prepared mechano-chemically. It is well known that the hexagonal wurtzite ZnO display three vibration modes in the Raman spectra: A_1 , E_1 and E_2 . A_1 and E_1 modes split into two modes, namely longitudinal optical (LO) and transverse optical (TO) components respectively, while E_2 (high) mode also consists of two modes of low and high frequency phonons [18]. The intense peak observed at 436.4 cm^{-1} for the undoped ZnO nanoparticles is known as the Raman-active dominant E_2 (high) mode, indicating that all prepared samples are of the hexagonal wurtzite phase ZnO [19]. The increase in the compressive stress on the sample causes the frequency shift to the red region of E_2 (high) phonon mode from 436.4 to 429.0 cm^{-1} . This is consistent with the XRD patterns as shown in Fig. 1. At a frequency of 329.6 cm^{-1} a peak associated with the $E_{2H}-E_{2L}$ mode can be observed. The third peak centred at 573.5 cm^{-1} represent two modes: A_1 (LO) and E_1 (LO) modes that are superimposed. This peak is believed to result from intrinsic defects in ZnO nanoparticles such as oxygen vacancy, zinc interstitial, or their complexes [20, 21]. The defects can also be observed in the PL spectra of the material which clearly confirms that the prepared samples are actually hexagonal wurtzite ZnO nanoparticles. It is observed in Fig. 4. that

all the graphs of the doped ZnO nanoparticles experiences a red-shift towards lower frequencies and they display the same pattern of mode. The intensity of the peaks decreases as dopants are introduced into the ZnO nanoparticles. The In-ZnO nanoparticles were observed to be favoured, hence the obtained frequencies are close to that of the undoped ZnO nanoparticles as compared to others. The position of the peaks obtained in Fig. 4., are in good agreement with what Schumm et al. [22] had obtained, where peaks at 329.5 cm^{-1} , 436.4 cm^{-1} and 573.5 cm^{-1} are for $E_{2H}-E_{2L}$, E_{2H} and A_1 & E_1 respectively for the excitation wavelength of 514.532 nm [23].

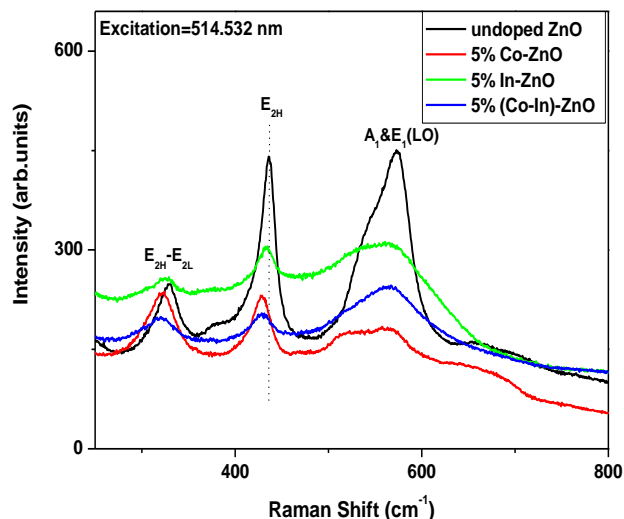


Fig. 4. Raman spectra of the undoped and 5% doped Co-ZnO, In-ZnO and (Co-In)-ZnO nanoparticles.

Ultraviolet-visible (UV-Vis) spectroscopy

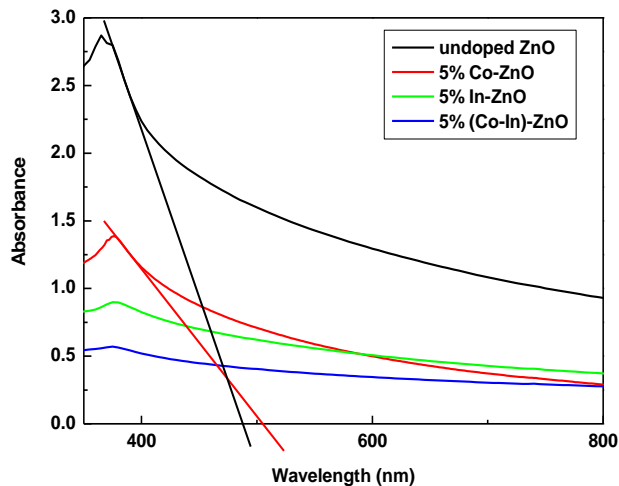
UV-Vis absorption spectra were recorded using Perkin-Elmer Lambda 750S UV-Vis spectrometer. This UV-Vis spectrometer was used to probe the optical band gap of the doped and undoped ZnO nanoparticles along the wavelength range of 350-800 nm. The calculations were done using the following equation [17]:

$$E_g = \frac{hc}{\lambda}, \quad (1)$$

here E_g is the energy band gap, h is the plank's constant ($6.626 \times 10^{-34} \text{ J}\cdot\text{s}$), c is the speed of light ($2.998 \times 10^8 \text{ m/s}$) and λ cut off wavelength in nm. The cut off wavelength was determined by extrapolating a straight line along the absorption edges through the wavelength axis. A point where the straight line intercepts the wavelength axis is our cut off wavelength, see Fig. 5. The E_g for undoped and doped ZnO nanoparticles was also calculated and presented in Table 2. The values obtained are ranging from 2.08 to 2.58 eV. The E_g of the co-doped (Co-In)-ZnO nanoparticles are much smaller than the Co-ZnO and In-ZnO nanoparticles. Previous literature by Wang et al. [24] shows that the bulk ZnO has the absorption at 387 nm in the UV-vis spectra which is obviously larger than that of the undoped ZnO nanoparticles (480 nm).

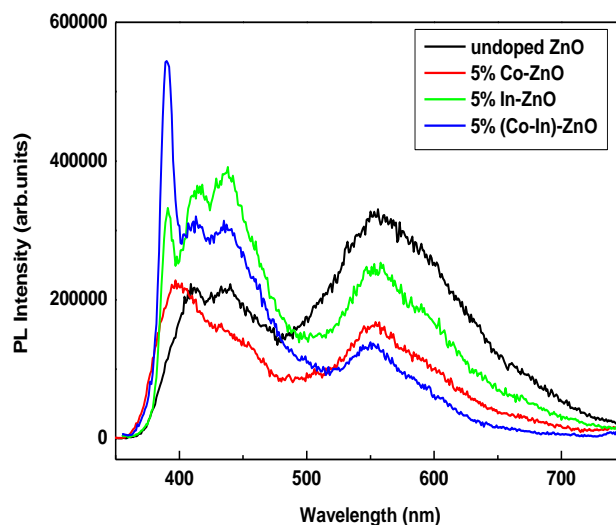
Table 2. The calculated Band Gap energy of the doped and undoped ZnO nanoparticles.

Sample	Doping (wt %)	Wavelength (nm)	Energy band gap (eV)
Bulk ZnO [24]	—	387.000	3.20
Undoped ZnO	0	479.917	2.58
Co-ZnO	5	509.830	2.43
In-ZnO	5	588.976	2.11
(Co-In)-ZnO	5	596.074	2.08

**Fig. 5.** UV-vis absorption spectra for undoped and 5% doped ZnO nanoparticles.

Photoluminescence (PL)

The NanoLog [iHR320 Horiba JOBINYVON] model of PL was used to collect data at room temperature. PL emission spectra of the undoped and doped In-ZnO, Co-ZnO and (In-Co)-ZnO nanoparticles are shown in **Fig. 6**. This spectrum was obtained with an excitation wavelength of 350 nm. The first near band edge ultraviolet (UV) emission peaks that appear in the PL spectra are for In-ZnO and (Co-In)-ZnO centred on 380 nm, which is attributed to the excitonic recombination. This is the recombination of an electron in the conduction band and a hole in the valence band [25]. A higher blue PL intensity is due to the presence of high number of ionised oxygen vacancy defects [26]. In-ZnO and (Co-In)-ZnO samples display similar trend in the behaviour of intensity as a function of wavelength even though the intensities are differing. This outcome may indicate that the ZnO nanoparticles synthesized by the high energy ball milling technique may possess high crystalline perfection. The undoped ZnO nanoparticles shows three defects, namely zinc interstitial (Zn_i), zinc vacancy (V_{Zn}) and oxygen vacancy (V_o) at 415 nm, 437 nm and 555 nm, respectively. Co-ZnO has two visible peaks along the 400 nm and 555 nm for valence band (VB) and V_o defects respectively. All the samples display the V_o and they range within 500-570 nm, which is the emission wavelength of green light [27].

**Fig. 6.** The Photoluminescence spectra for 5% doped and undoped ZnO nanoparticles at the excitation wavelength of 350 nm

Conclusion

ZnO nanoparticles were successfully synthesized using high energy ball milling technique. The XRD characterization confirms that the prepared samples were of hexagonal wurtzite ZnO nanoparticles. SEM images further validate the formation of spherical granular ZnO nanoparticles. The Raman spectra of the undoped ZnO nanoparticles displays a very strong peak of E_2 (high) that clearly indicate that the prepared material was of a hexagonal wurtzite ZnO phase. As the dopants were introduced in the ZnO nanostructure samples, a red shift was experienced. The PL spectra indicated that doped ZnO nanoparticles have a strong UV emission peak at 380 nm and green emission band at 555 nm. Doped samples show very obvious peaks in the visible region of the spectrum. These peaks are an indication of defects in the original ZnO nanoparticles. From the UV-Vis results it can be concluded that as dopants are introduced into the ZnO structure the band gap decreases, which further decrease with co-doping the ZnO nanoparticles with Co-In.

Acknowledgements

The authors are grateful with the financial support from UL, NRF and IBSA. National Centre for Nano-Structures Materials at CSIR is thanked for characterisation facilities. Mpho Maswanganye is thanked for valuable discussions.

Author's contributions

Conceived the plan: TEM; Performed the experiments: MFM, BWM; Data analysis: MFM, TEM, BWM; Wrote the paper: MFM, TEM, BWM. Authors have no competing financial interests.

References

- Rani, G.; Sahare, P.D.; *J. Mater. Sci. Technol.*, **2013**, 29, 1035. DOI: 10.1616/j.jmst.2013.08.015
- Soitah, T. N.; Chunhui, Y.; Liang, S.; *Sci. Adv. Mater.*, **2010**, 2, 534. DOI: 10.1166/sam.2010.1120

3. Kind, H.; Yan, H. Q.; Messer, B.; Law, M.; Yang P. D.; *Adv. Mater.*, **2002**, 14, 158.
4. Chakraborty, A.; Mondal, T.; Bera, S. K.; Sen, S. K.; Ghosh, R.; Paul G. K.; *Mater. Chem. Phys.*, **2008**, 112, 162.
5. Li, Y.; Cheng, C.; Dong, X.; Gao, J.; Zhang H.; *J. Semicond.*, **2009**, 30, 38.
6. Djerdj, I.; Jaglicic, Z.; Arcon, D.; Niederberger M.; *Nanoscale*, **2010**, 2, 1096.
7. Dinesha, M. L.; Jayanna, H. S.; Mohanty, S.; Ravi, S.; *J. Alloys Compd.*, **2010**, 490, 618.
8. N'emeth, J.; Rodriguez-Gattorno, G.; Diaz, D.; V'azquez-Olmos, A.R.; D'ek'any, I.; *Langmuir*, **2004**, 20, 2855.
9. Singh, J.; Mohapatra, S.; *Adv. Mat. Lett.*, **2015**, 6, 924.
10. Spanhel, L.; Anderson, M.A.; *J. Am. Chem. Soc.*, **1991**, 113, 2826.
11. Maswanganye, M. W.; Rammutla, K. E.; Mosuang, T. E.; Mwakikunga, B. W.; Bertrand, S. T.; Maaza, M.; *Adv. Mat. Lett.*, **2017**, 8(1), 37.
12. Liu, J.; Luo, T.; Meng, F.; Qian, K.; Wan, Y.; Liu, J.; *J. Phys. Chem. C*, **2010**, 114, 4887.
13. Shannon, R.; *Acta Cryst. A*, **1976**, 32, 751.
14. Zhang, Y.; Mu, J.; *Nanotechnology*, **2007**, 18, 075606.
15. Zak, A. K.; Majid, W. H. A.; Abrishami, M. E.; Yousefi, R.; *Solid State Sci.*, **2011**, 13, 251.
16. Fan, Z.; Lu, J. G.; *J. Nanosci. Nanotechnol.*, **2005**, 5, 1561.
17. Sharma, D.; Sharma, S.; Kaith, B. S.; Rajput, J.; Kaur, M.; *App. Surf. Sci.*, **2011**, 257, 9661.
18. Mhlongo, G. H.; Motaung, D. E.; Nkosi, S. S.; Swart, H. C.; Malgas, G. F.; Hollie, K. T.; Mwakikunga, B. W.; *App. Surf. Sci.*, **2014**, 293, 62.
19. Damen, T. C.; Porto, S. P. S.; Tell, B.; "Raman Effect in Zinc Oxide," *Phys. Rev.*, **1966**, 142, 570.
20. Panda, S. K.; Jacob, C.; *Appl. Phys. A*, **2009**, 96, 805.
21. Wang, Y.; Li, X.; Wang, N.; Quan, X.; Chen, Y.; *Sep. Purif. Technol*, **2008**, 62, 727.
22. Schumm, M.; Geurts, J.; Neder, R.; *Dissertation, Uniersität Würzburg, Germany*, **2008**, 45-53.
23. Kabongo, G. L.; Mhlongo, G. H.; Malwela, T.; Mothudi, B. M.; Hillie, K. T.; Dhlamini, M. S.; *J. Alloys Compd.*, **2014**, 591, 156.
24. Wang, C.; Shen, E.; Wang, E.; Gao, L.; Kang, Z.; Tian, C.; Lan, Y.; and Zhang, C.; *Mater. Lett.*, **2005**, 59, 2867.
25. Chen, J.; Li, J.; Xiao, G.; Yang, X.; *J. Alloys Compd.*, **2011**, 509, 740.
26. Motaung, D. E.; Makgwane, P. R.; Ray, S. S.; *Mater. Lett.*, **2015**, 139, 475.
27. Willander, M.; Nur, O.; Sadaf, J. R.; Qadir, M. I.; Zaman, S.; Zainelabdin, A.; Bano, N.; Hussain, I.; *Materials*, **2010**, 3, 2643.

(a) Scientific article

1. Sanchez, C.; Belleville, P.; Popall, M.; Nicole, L; *Chem. Soc. Rev.*, **2011**, 40, 696.
DOI: [10.1039/c0cs00136h](https://doi.org/10.1039/c0cs00136h)

(b) Book

2. Tiwari, A.; Kobayashi, H. (Eds.); *Responsive Materials and Methods*; Wiley: USA, **2013**.
DOI: [10.5185/sbm-2010-01](https://doi.org/10.5185/sbm-2010-01)

(c) Book Chapter

3. Nam, K.; Kishida, A. Application of the Collagen as Biomaterials, In *Biomedical Materials and Diagnostic Devices*; Tiwari, A.; Ramalingam, M.; Kobayashi, H.; Turner, A.P.F. (Eds.); Wiley: USA, **2012**, pp. 3-18.
DOI: [10.1021/bk-2010-1045.ch001](https://doi.org/10.1021/bk-2010-1045.ch001)